AIMS Mathematics, 8(4): 8332–8348.
DOI: 10.3934/math.2023420
Received: 12 September 2022
Revised: 31 December 2022
Accepted: 09 January 2023
Published: 02 February 2023

http://www.aimspress.com/journal/Math

*Research article*

# Numerical solution for heat transfer in a staggered enclosure with wavy insulated baffles

**Rashid Mahmood[1], Nusrat Rehman[1], Afraz Hussain Majeed[1], Khalil Ur Rehman[2,3,*] and Wasfi Shatanawi[2,4]**

[1] Faculty of Basic Applied Sciences, Department of Mathematics, Air University, PAF Complex E-9, Islamabad 44000, Pakistan
[2] Department of Mathematics and Sciences, College of Humanities and Sciences, Prince Sultan University, Riyadh 11586, Saudi Arabia
[3] Department of Mathematics, Air University, PAF Complex E-9, Islamabad 44000, Pakistan
[4] Department of Mathematics, Faculty of Science, The Hashemite University, P.O Box 330127, Zarqa 13133, Jordan

* **Correspondence:** Email: kurrehman@psu.edu.sa.

**Abstract:** The present study contains examination on partial differential equations narrating heat transfer aspects in magnetized staggered cavity manifested with wavy insulated baffles. The nanoparticles namely Aluminium oxide are suspended in the flow regime within staggered enclosure having purely viscous fluid. The flow is modelled mathematically in terms of partial differential equations and the finite element is used to discretized the flow differential equations. The effects of several parameters such as Hartmann number $(0 \leq Ha \leq 100)$, Volume fraction $(0.00 \leq \phi \leq 0.08)$, Rayleigh number $(10^3 \leq Ra \leq 10^5)$, and angle of inclinaton $(0^o \leq \gamma \leq 60^o)$ on the thermal flow and distribution of nanomaterials for natural convection are inspected. It is calculated how much Ha will affect velocities and isotherms wit h $Ra = 10^4$ and $\phi = 0.02$. With Ha = 20 and $\phi$ = 0.02, the effect of Ra on velocity and isotherms is also estimated. The average Bejan number and average Nusselt number against Hartmann number are investigated. When the walls move in an opposite direction, line graphs of velocity distribution are created for both the u and v components. The presence of Hartmann number leads to increase in Bejan number while, opposite behavior can be observed in case of average Nusselt number. When the volume fraction is large, the velocity increases significantly. The flow strength is greater when the Rayleigh number is smaller. On the other hand, as Ra drops, or when $Ra = 10^4$, flow strength drops.

**Keywords:** heat transfer; staggered cavity; nanomaterials; insulated baffles; inclined MHD; finite element method
**Mathematics Subject Classification:** 35A25, 65MO6, 76D05, 76M10

## Nomenclature

| | |
|---|---|
| $C_p$ | Specific heat ($kjkg^{-1}K^{-1}$) |
| $B_o$ | Magnetic induction ($T$) |
| $p$ | Pressure ($Nm^{-2}$) |
| $S_{Mag}$ | Magnetic entropy ($Jm^{-3}s^{-1}K^{-1}$) |
| $S_{Ther}$ | Thermal entropy ($Jm^{-3}s^{-1}K^{-1}$) |
| $S_{Vis}$ | Viscous entropy ($Jm^{-3}s^{-1}K^{-1}$) |
| $S_i$ | Total entropy ($Jm^{-3}s^{-1}K^{-1}$) |
| $T$ | Temperature ($K$) |
| $x, y$ | Non-dimensional coordinates |
| $u, v$ | Non-dimensional velocities (m$s^{-1}$) |
| $\Delta T$ | Temperature gradient |
| $k_b$ | Boltzmann's constant (J.$k^{-1}$) |
| $Ha$ | Hartmann number |
| $H$ | Cavity height ($m$) |
| $Ra$ | Rayleigh number |
| $Be$ | Bejan number |
| $Nu_{avg}$ | Average Nusselt number |
| $P_r$ | Prandtl number |
| $d_s$ | nanoparticles diameter ($m$) |
| $k$ | Thermal conductivity ($Wm^{-1}k^{-1}$) |
| $Be$ | Bejan number |
| $c$ | Cold side |
| $s$ | solid |
| $o$ | Reference |
| $avg$ | Average |

## Greek symbols

| | |
|---|---|
| $\alpha$ | Thermal diffusivity ($m^2s^{-1}$) |
| $\beta$ | Expansion coefficient ($K^{-1}$) |
| $\phi$ | Volume fraction (%) |
| $\mu$ | Viscosity ($kgm^{-1}s^{-1}$) |
| $\rho$ | Density (kg.$s^3$) |
| $\psi$ | Distribution irreversibility ratio |
| $\sigma$ | Electrical conductivity ($\Omega^{-1}m^{-1}$) |
| $\gamma$ | Inclination (rad) |

**Subscripts**

| | |
|---|---|
| $f$ | fluid |
| $nf$ | nanofluid |
| $h$ | Fluid hot side |

## 1. Introduction

To examine the heat transfer aspects in various configuration having thermal engineering standpoints, the computational fluid dynamics (CFD) has played an essential role in overcoming the limitations faced by analytical and experimental approach. In CFD, Navier-Stokes has traditionally served as the governing equation. Over the past few decades, research on the fluid flow in Lid Driven Cavities (LDCs) has been a cornerstone of CFD, especially for developing innovative numerical schemes [1–7]. Nevertheless, double-driven staggered LDC has recently gained considerable attention from researchers. For anti-parallel as well as parallel lids motions, Kalita and Gogoi [8] performed study on the flow inside a two-sided staggered lid-driven hollow. The flow differential equations for this problem leading to the extended eigenvalue issue, were discretized using second and a fourth order temporally and spatially accurate compact scheme respectively. For various grids, estimates of essential parameters were discovered, and an intensive grid convergence examination was conducted to correctly identify them. The numerical results towards the critical Reynolds number were compared to existing ones, and first-rate agreement was found in all situations. The fluid flow in square cavity is mathematically modelled by Indukuri and Maniyeri [9]. In this attempt, finite volume method along with staggered grid scheme was used. For the situation of finite wall motion, the constructed computer model was first validated against the results of other researchers. After that, numerical simulations were run for upper wall oscillations towards Re and frequency combinations. Following such results, an ideal frequency was established, and then simulations were run to investigate the vortex behavior for parallel and anti-parallel wall oscillations. They determined from these simulations that Re = 1000 was a good operating range for well mixing within enclosure both for anti-parallel and parallel wall oscillations.

Nanotechnology is frequently used in industry because nanoscale materials have remarkable chemical and physical capabilities. Nanofluids are fluids with nanoscale particles added to them, and Choi was the first to use them in 1995. Natural convention, thermal conductivity, boiling heat transfer and convective heat transfer are some of the experimental and numerical investigations on nanofluids. Öztop and Abu-Nada [10] used nanofluids and several types of nanoparticles to examine the heated fluid flow towards an enclosure. The heater was flush placed and had a finite length on the left wall. The right vertical wall had a lower temperature than the heater, whereas the other walls were kept insulated. The finite volume method was used to solve the flow equations. Nanoparticles of various sorts were tried. For the whole range of Rayleigh numbers, the volume fraction of nanoparticles was observed to raise the mean Nusselt number. Heat transfer increases as the height of the heater rises. When employing nanofluids, it was discovered that the heater placement impacts the flow and temperature fields. The heat transfer increase with nanofluids was found to be more pronounced at higher aspect ratio. Besides this, Hinatsu and Ferziger [11] described a composite multigrid approach and how it was used to a geometrically difficult flow. The internal endpoint conditions treatment within a composite multigrid approach for a 1D model equation was thoroughly explained. The flow

equations were discretized using a staggered grid methodology and its effectiveness was demonstrated using lid-driven cavity flows. The double driven staggered lid driven cavities is a somewhat modified variant of the modest two-sided lid driven cavities, which was presumably initially extensively explored by Kuhlmann et al. [12] The flow field in rectangular enclosures was examined experimentally as well numerically in this article. Here, flow was created by tangentially stirring two opposing walls. The 2D flow was discovered to be not always be unique. It comprises of two distinct co-rotating vortices close to the stirring walls for low Reynolds numbers. If the difference in sidewall Reynolds numbers is considerable, we may have unstable flow. A second two-dimensional flow exists when aspect ratio is above the two or we have high Re. It appears as a single vortex that fills the entire cavity. In the current experiment, this was the preferable state. The instability was subcritical when they differed. The mechanism of destabilization was shown to be identical to the destabilization appliance operational in the strained vortices elliptical instability, based on 3D flow and energy analysis. The related examination in this regard can be reached in Ref. [13]. A backward-facing step and a lid-driven cavity are combined in a two-sided lid staggered cavity. It also possesses all of the key characteristics of a complicated geometry. Zhou et al. [14] and Nithiarasu & Liu [15] has introduced and analyzed non rectangular lid-driven cavities (two sided) as a potential benchmark challenge. Wavelet-based discrete singular convolution was utilized by Zhou et al. [14] to provide an answer for flow in a staggered two-sided lid-driven cavity. Nithiarasu and Liu [15] tackled a similar issue by utilizing the artificial compressibility and characteristic based split (CBS) scheme.

Alsallami et al. [16] address the aspects of entropy generation for time-independent second-grade nanomaterials for disc flow that exhibits rotational behaviors. According to this study, the Bejan number and entropy generation exhibit the same pattern for the temperature and concentration difference parameters, but the fluid and magnetic parameters exhibit the opposite tendency. The focus of the Usman et al. [17] research is forced convection with a high Reynolds number of a water-alumina-based nanofluid in a square cavity with a rotating disc revolving at a constant speed.

The use of a roughened surface to improve passive heat transmission in a duct or channel is one of the most successful methods. The creation of recirculation, flow separation, and impingement is induced by a baffled surface. The flow impingement in type of a high velocity jet is essentially liable for heat transfer improvement because of its profoundly compelling thermal boundary layer aggravation. A few scientists have examined impacts of rib geometries and baffle on the pressure drop, heat transfer enhancement and warm execution. Impact of three-sided wavy baffles on fluid flow and heat qualities in a channel is numerically examined by Eiamsa et al. [18] Al-Rashed et al. [19] considered the characteristics of thermal flow and entropy generation inside a 3D cavity loaded up with CNT (carbon nanotube)-water nanofluids for a scope of Rayleigh numbers from 10E3 to 10E5. Rehman et al. [20] provided a numerical results based on finite element method for flow fields in a staggered cavity.

Reddy et al. [21] carry out a numerical analysis of the magneto-free convective flow in a square cavity with internal heat generation. It has been discovered that as the Rayleigh number's nanoparticle volume fraction rises, the global entropy generation declines. The flow of a hybrid nanofluid across a porous medium was explored numerically by Bhatti et al. [22] In a microchannel with a porous medium, Bhatti et al. [23] establish a mathematical model for laminar, steady-state, fully developed viscoelastic natural convection electro-magnetohydrodynamic (EMHD) flow. The third-grade fluid and the strong magnetic field impact greatly impede the mobility of the fluid.

The novelty of present attempt is the examination of thermal flow regime within staggered

enclosure manifested with insulated wavy baffle. The flow field is further interacted with magnetic field and nanoparticles are suspended in the fluid. The simulation has done by implementing the Galerkin finite element scheme. Influence of Hartmann number, Rayleigh number, inclined angle and volume fraction of aluminum oxide on thermal flow are considered. The structure of draft is as follows: Section-1 holds limited motivational literature survey. The problem statement is debated in Section-2. Section-3 is devoted as Entropy generation. The adopted numerical scheme is debated in Section-4. The obtained results are analyzed in Section-5. The key outcomes of present attempt are offered in Section-6.

## 2. Mathematical description

A mathematical model for the inclined MHD nanofluid in a staggered enclosure with insulated baffles has been considered. The schematic diagram of the given problem is shown in Figure 1a. The vertical walls are thought to be heated while the horizontal walls have been taken as cold. To investigate the steady, incompressible and laminar flow field in staggered cavity the mathematical description of continuity, momentum, and heat equation [24] is as follows:

$$\frac{\partial u}{\partial x}+\frac{\partial v}{\partial y}=0, \tag{1}$$

$$u\frac{\partial u}{\partial x}+v\frac{\partial u}{\partial y}=-\frac{\partial p}{\partial x}+\frac{\mu_{nf}}{\rho_{nf}\,\alpha_f}\left(\frac{\partial^2 u}{\partial x^2}+\frac{\partial^2 u}{\partial y^2}\right)+\frac{\sigma_{nf}}{\sigma_f}Pr_f Ha^2(vsin\gamma cos\gamma-usin^2\gamma), \tag{2}$$

$$u\frac{\partial v}{\partial x}+v\frac{\partial v}{\partial y}=-\frac{\partial p}{\partial y}+\frac{\mu_{nf}}{\rho_{nf}\,\alpha_f}\left(\frac{\partial^2 v}{\partial x^2}+\frac{\partial^2 v}{\partial y^2}\right)+\frac{(\rho\beta)_{nf}}{\rho_{nf}\,\beta_f}R\alpha_f Pr_f T+\frac{\sigma_{nf}}{\sigma_f}Pr_f\,Ha^2(usin\gamma cos\gamma-vcos^2\gamma), \tag{3}$$

$$u\frac{\partial T}{\partial x}+v\frac{\partial T}{\partial y}=\frac{\alpha_{nf}}{\alpha_f}\left(\frac{\partial^2 T}{\partial x^2}+\frac{\partial^2 T}{\partial y^2}\right). \tag{4}$$

Solid particles and base fluids are used to determine the density and thermal expansion coefficient of the nanofluid, as well as the coefficient of specific heat [24].

$$\rho_{nf}=(1-\varphi)\rho_f+\varphi\rho_s, \tag{5}$$

$$(\rho\beta)_{nf}=(1-\varphi)(\rho\beta)_f+\varphi(\rho\beta)_s, \tag{6}$$

$$(\rho c_p)_{nf}=(1-\varphi)(\rho c_p)_f+\varphi(\rho c_p)_s, \tag{7}$$

$$\frac{\mu_{nf}}{\mu_f}=\frac{1}{(1-\varphi)^{2.5}}. \tag{8}$$

It is evident that Eq (8) relates to the Brinkman model in terms of viscosity. The Maxwell model is used to calculate electric conductivity [25].

$$\frac{\sigma_{nf}}{\sigma_f}=1+\frac{3\left(\frac{\sigma_s}{\sigma_f}-1\right)\varphi}{\left(\frac{\sigma_s}{\sigma_f}+2\right)-\left(\frac{\sigma_s}{\sigma_f}-1\right)\varphi}, \tag{9}$$

for thermal conductivity Lee et al. [26] model is used.

$$k_{nf}=k_f\left(1+\frac{k_s A_s}{k_f A_f}+Ck_s\mathrm{Pe}\frac{A_s}{k_f A_f}\right). \tag{10}$$

Here C = 2.5× $10^4$. The following are the values for the parameter Pe and $\frac{A_s}{A_f}$:

$$\text{Pe} = \frac{u_s\, d_s}{\alpha_f},\ \frac{A_s}{A_f} = \frac{d_s}{d_f}\ \frac{\epsilon}{1-\epsilon}. \tag{11}$$

As shown above, a water molecule's diameter is represented by $d_f$, measured in 2A, and the solid nanoparticles diameter is own as $d_s$. By using the parameter $u_s$, Brownian motion velocity (BMV) of the nanoparticles, which is a function of temperature, is determined which is given by [27], we can determine the BMV of the nanoparticles.

$$u_s = \frac{2k_bT}{\pi\mu_f {d^2}_s}, \tag{12}$$

Boltzmann's constant is represented by $k_b$.

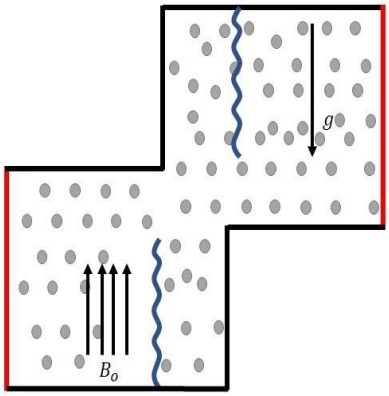


**Figure 1(a)**. Physical domain of the problem.

In this case, the boundary conditions are as follows:

i) $T_h$ = 1, at the vertical walls (red color);
ii) $T_c$ = 0, except the vertical walls (black color);
iii) $\frac{\partial T}{\partial n}$ = 0, at the wavy baffles;
iv) The no-slip criterion is implemented as u = v = 0 at all the walls.

## 3. Entropy generation

Analyzing irreversibility involves adding conjugated fluxes and produced forces to measure local entropy production. The non-dimensional local entropy in a convective practice with the influence of a magnetic field is given by: The measurement of local entropy production derived by adding conjugated fluxes and produced forces is referred to as irreversibility analysis. The non-dimensional local entropy production in a convective process and under the effect of a magnetic field is given by:

$$Si = \frac{k_{ff}}{k_f}\left[\left(\frac{\partial T}{\partial x}\right)^2 + \left(\frac{\partial T}{\partial y}\right)^2\right] + \psi\left[2\left(\frac{\partial u}{\partial x}\right)^2 + 2\left(\frac{\partial v}{\partial y}\right)^2 + \left(\frac{\partial u}{\partial y} + \frac{\partial v}{\partial x}\right)^2\right] + \frac{\sigma_{ff}}{\sigma_f} Ha^2\psi(usin\gamma - vcos\gamma)^2, \tag{13}$$

$$Si = S_{Ther} + S_{Vis} + S_{Mag}, \tag{14}$$

where,

$$S_{Ther} = \frac{k_{ff}}{k_f}\left[\left(\frac{\partial T}{\partial x}\right)^2 + \left(\frac{\partial T}{\partial y}\right)^2\right], \tag{15}$$

$$S_{Vis} = \psi\left[2\left(\frac{\partial u}{\partial x}\right)^2 + 2\left(\frac{\partial v}{\partial y}\right)^2 + \left(\frac{\partial u}{\partial y} + \frac{\partial v}{\partial x}\right)^2\right], \tag{16}$$

$$S_{Mag} = \frac{\sigma_{ff}}{\sigma_f} Ha^2\psi(usin\gamma - vcos\gamma)^2. \tag{17}$$

Here $Si$, $S_{Ther}$, $S_{Vis}$ and $S_{Mag}$represents the local entropy generation, heat transfer irreversibility, entropy generation due to viscous irreversibility and the irreversibility due to magnetic field respectively. In Eq (13) the formula for distribution irreversibility ratio ($\psi$) is given below in Eq (18).

$$\psi = \frac{\mu_{ff}T_0}{k_f}\left(\frac{\alpha_f}{H\Delta T}\right)^2. \tag{18}$$

Here $T_o$ represents the average temperature calculated as $T_o = \frac{T_h + T_c}{2}$.

In addition, the non-dimensional Bejan number $(Be)$ described as the ratio of thermal entropy $S_{Ther}$ and local entropy $Si$ which is given as $Be = \frac{S_{Ther}}{Si}$. In order to achieve accuracy, we use both rectangular and triangular elements to create a hybrid mesh (shown in Figure 1b). Using various nanofluids, Figure 1c illustrates vertical velocity profile along the middle of the cavity. The results show the good agreement with Öztop work [10].

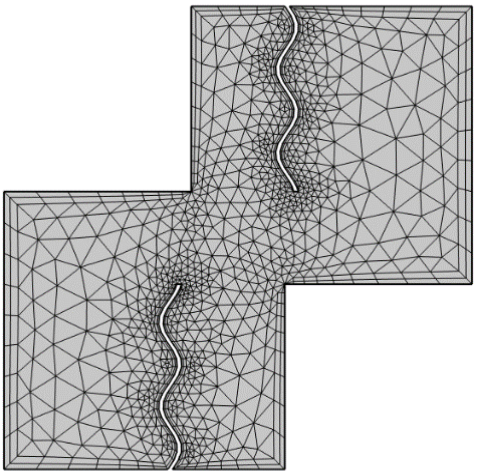

**Figure 1(b).** Hybrid mesh at coarse level.

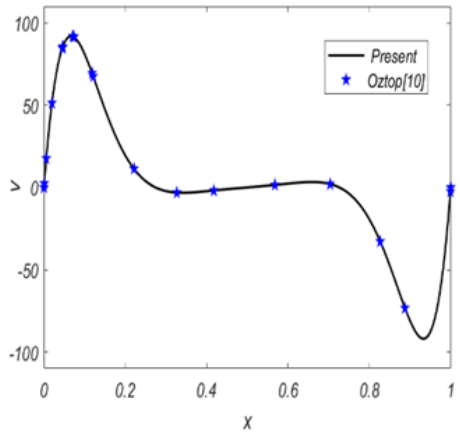


**Figure 1(c).** Comparison of present study with Öztop [10].

## 4. Numerical approach and validation

It is important to note that the energy equation and momentum equation cannot be solved analytically due to the equation's nonlinearity and the plastic viscosity of the non-Newtonian fluid; hence, a numerical scheme was used to solve the equations. In order to determine a more accurate approximation, the finite element strategy is used. One of the most impressive numerical techniques and commonly utilized way to deal the boundary value issues is the finite element method. The underlying discrete nonlinear system of equations was linearized using the Newton's method, and the linearized inner systems were solved with PARDISO, a direct solver that uses LU matrix factorization, which minimizes the number of iterations required to get the appropriate level of convergence. As a result, the number of iterations required is reduced [28–36]. This method can be used to describe and simulate many physical processes in interconnect architectures. The six key steps in the finite element approach are as follows:

i) Domain discretization;
ii) Create local finite element equations;
iii) Assemble local contributions to obtain global matrix;
iv) Incorporate the boundary and/or initial conditions;
v) Solve the developed system;
vi) Post Processing.

In order to achieve accuracy, we used both rectangular and triangular elements to create a hybrid mesh shown in Figure 1b.

## 5. Results and discussion

The viscous fluid flow within a staggered enclosure is investigated numerically by using finite element method. An inclined magnetic field is applied along with the suspended nanoparticles in the flow regime. Table 1 reveals the properties of nanofluid particle and base fluid. The outcomes are detailed by using contour plots and line graphs. In detail, for varied values of volume fraction $(\phi)$ and with constant Hartmann number ($Ha = 20$) and Ra=$10^4$, the effects on velocity (left) and isotherms (right) are shown in Figure 2. For $\phi$ =0.00 indicates the base fluid.

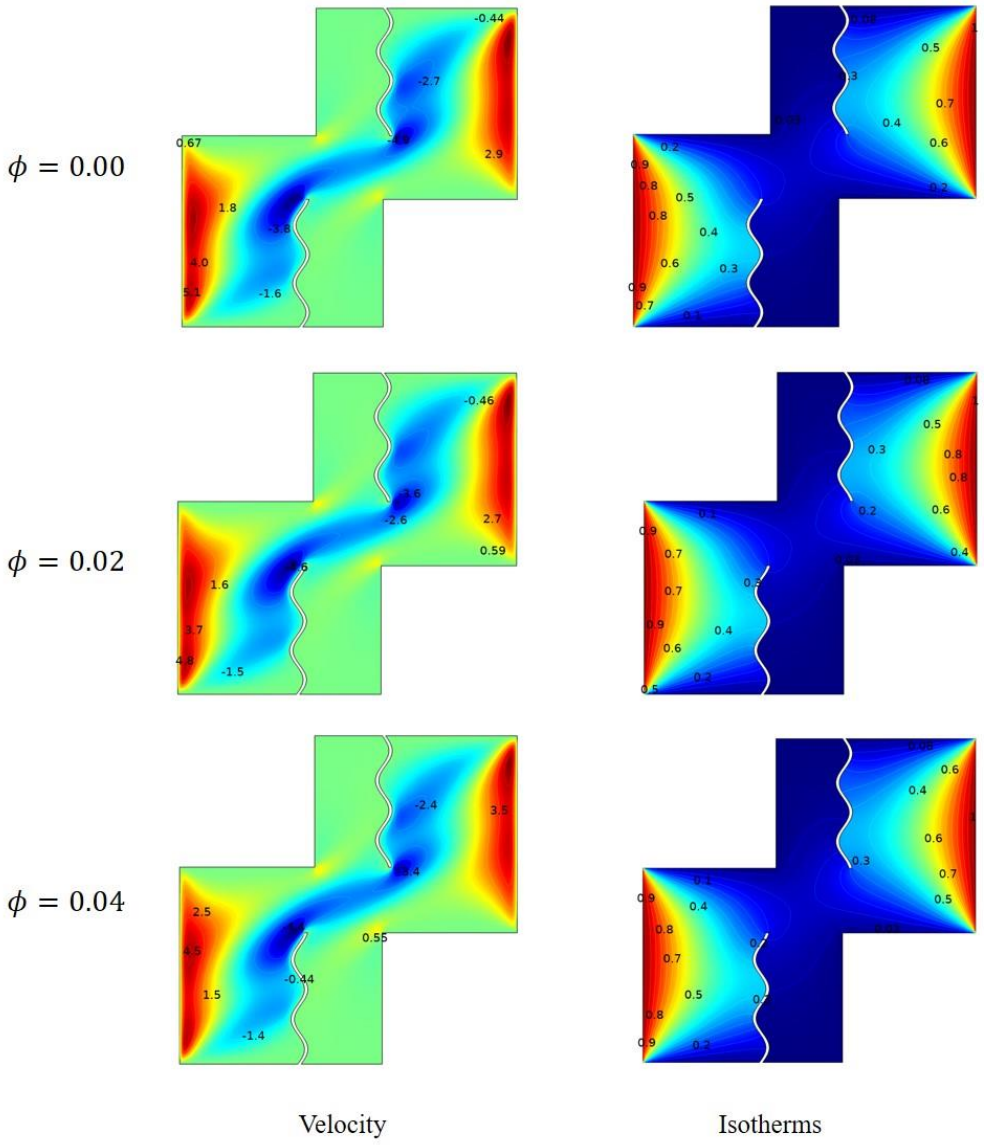


**Figure 2.** Impact on velocity and isotherms for different $\phi$ with $Ha = 20$ and $Ra = 10^4$.

**Table 1.** Physical characteristics of the base fluid and nano-particles.[24].

| Nano-particles | ρ | $C_p$ | k | β |
|---|---|---|---|---|
| | $kgm^{-3}$ | $Jkg^{-1}K^{-1}$ | $Wm^{-1}K^{-1}$ | $K^{-1}$ |
| $H_2O$ | 997.1 | 4179 | 0.613 | 21E-5 |
| $Al_2O_3$ | 3970 | 765 | 25 | 0.85E-5 |

It can be seen that the when the value of volume fraction increases, isotherms move towards to the heater wall. Clearly, heated fluid strength is increased towards higher volume fraction $\phi$ of nanoparticles, based on the isotherms. The magnitude of velocity enhanced as well towards $\phi$ of nanoparticles. Figure 3 shows the Impact on velocity and isotherms for different $Ra$ with fixed

$Ha = 20$ and $\phi$= 0.02.

When the Rayleigh number is lower, the flow strength is higher. Conversely, flow strength decreases for lower values of Ra for instance $Ra = 10^4$. Isotherms show almost same distribution due to closer value of thermal conductivity of $Al_2O_3$ given in Table 1. In Figure 4, the impact of velocity (left) and isotherms (right) for different Hartman number (Ha) with fixed Ra=$10^4$ and $\phi$= 0.02 is described. It can be seen that when the value of $Ha$ increases the cell are very close to each other. By examining how nanoparticles influence flow and isotherms, it becomes apparent that nanoparticles influence both. Line graphs of velocity distribution are constructed for both u and v components when the walls move antiparallel. Figure 5 illustrates in more detail the u-velocity and v-velocity line graph studies towards $Ha = 20$ and $Ra = 10^4$ with different values of $\phi$ and $\gamma$. It can be observed that all the u-velocity and v-velocity graphs are starts from zero, the graphs are increasing first, then sharply decreases after that again gradually decreasing. It can also be observed that when the value of volume fraction ($\phi$) increases, the graph of u and v velocities decreases. In short for u -velocity, a small sinusoid fluctuation is found.

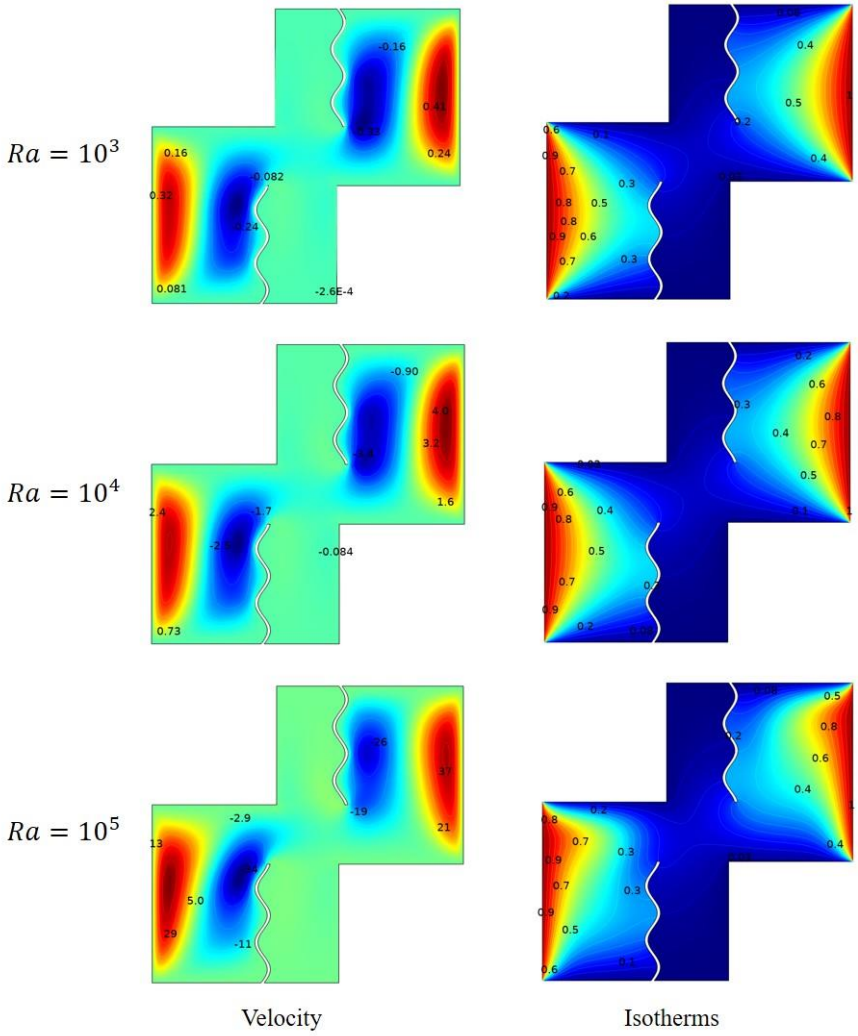


**Figure 3**. Influence of $Ra$ on velocity and isotherms with $Ha = 20$ and $\phi = 0.02$.

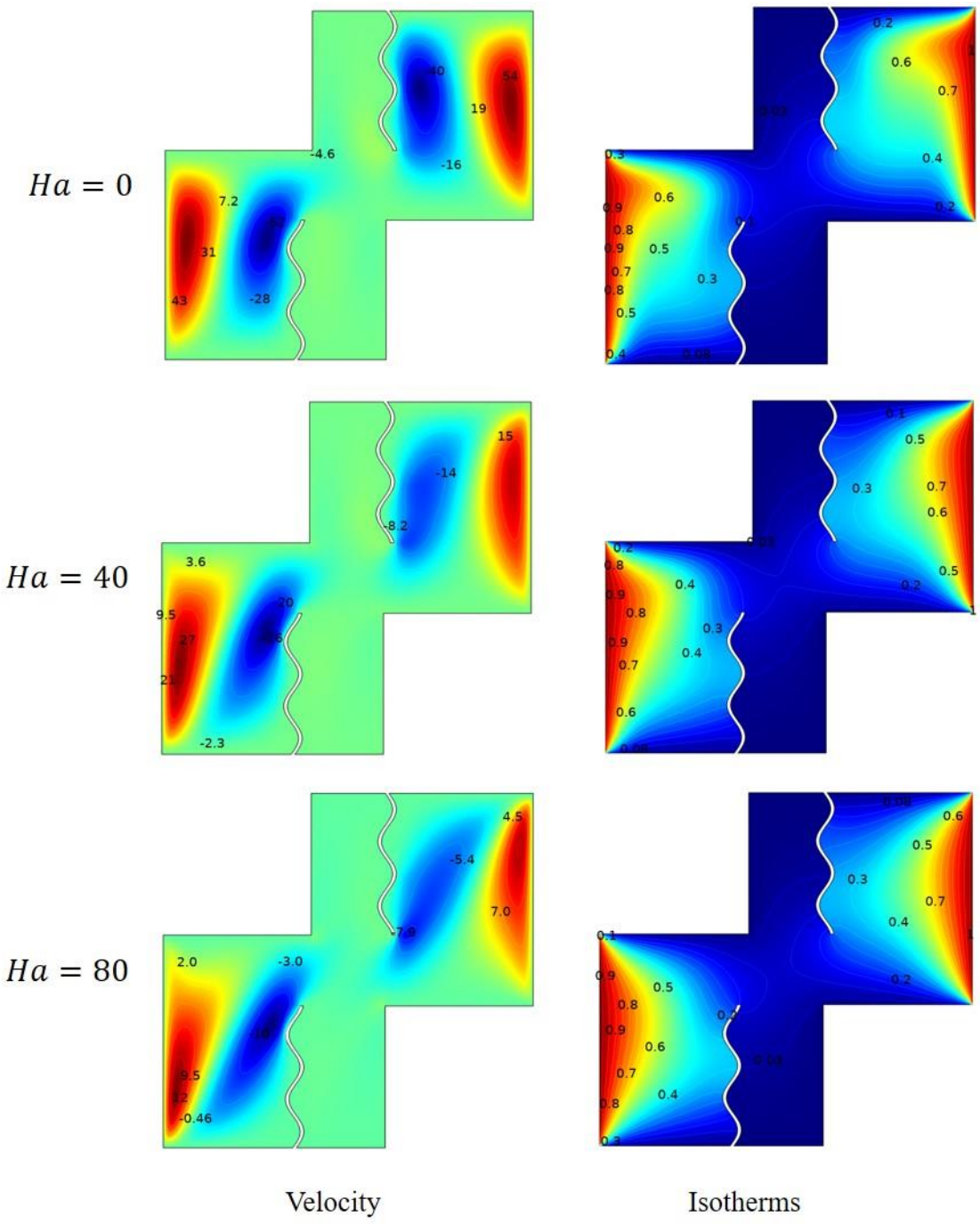


**Figure 4**. Influence of $Ha$ on velocity and isotherms with $Ra = 10^4$ and $\phi = 0.02$.

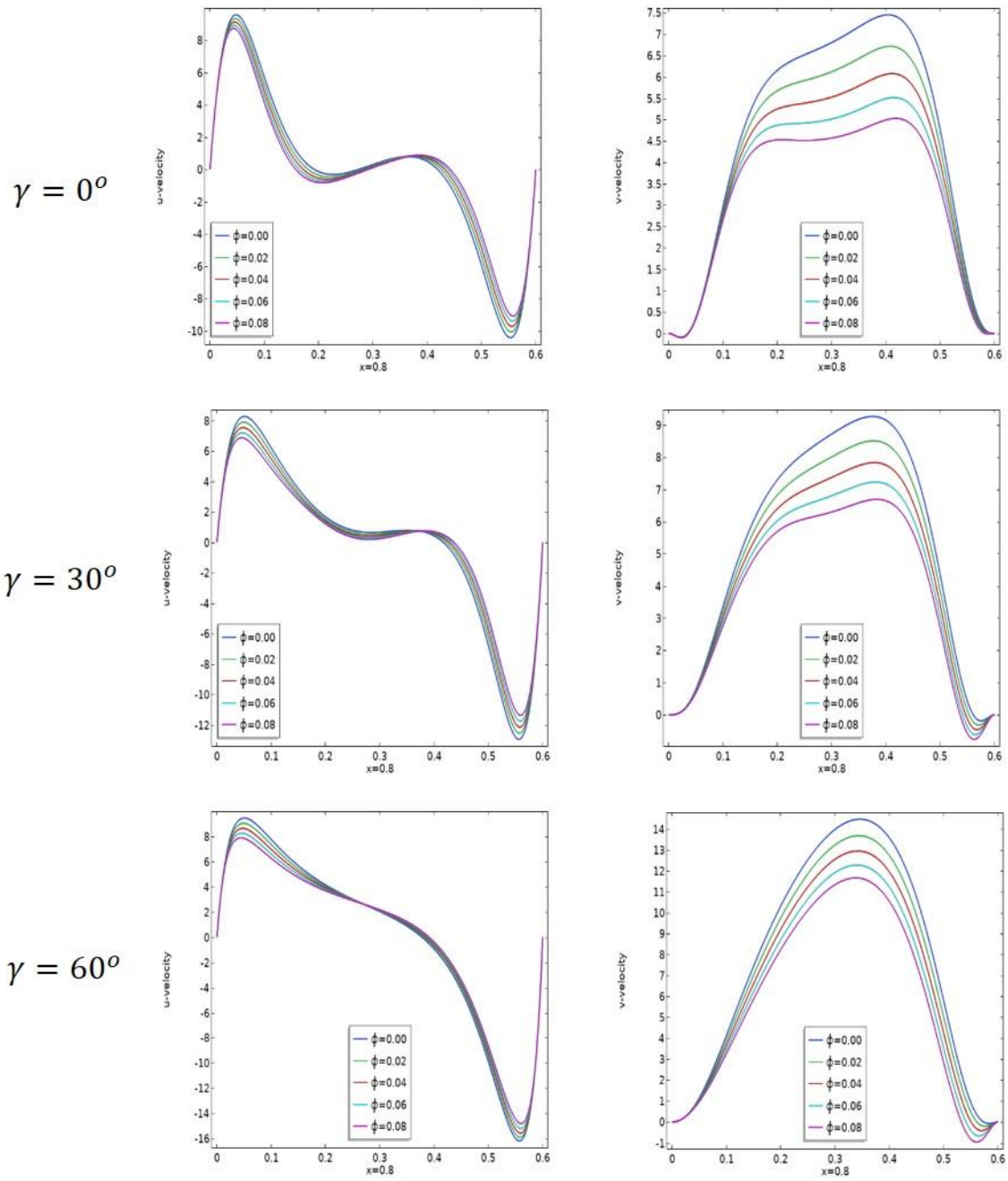


**Figure 5**. Impact on velocity components for different $\phi$ with $Ha = 20$ and $Ra = 10^4$.

For v-velocity graphs, it can easily be found that the velocity is greater on center and minimum on surfaces, gradually obtaining the shape of parabola. For $\gamma$=60°, a perfect parabola shape is obtained. The effects of various values of volume fraction $(\phi)$ and inclination angle $\gamma$ on Bejan number with Ha=20 and $Ra = 10^4$ are shown in Figure 6. It can be seen that for $\gamma$=0° and $\gamma$=30°, the curves show almost the same behavior. While, in case of $\gamma$=60°, the curve is changing its shape. This indicates that the Bejan number will be higher for a lower volume fraction $\phi$. The Bejan number accomplishes its greatest worth inside the above half cavity, though for most $\phi$ , it acquires the minimum value in the bottom half cavity. Additionally, it is clear that the graphs of u and v velocities grow as the volume fraction $\phi$ increases. Figure 7 show the impact on average Bejan and average Nusselt number against Ha. In Figure 7a the graph of Bejan number against $Ha$ is analysed and in Figure 7b the graph of

$Nu_{avg}$ against $Ha$ are analysed. In case of Bejan number, the curves are increasing and then intersect each other at Ha=30 while in case of average Nusselt number the curves are decaying.

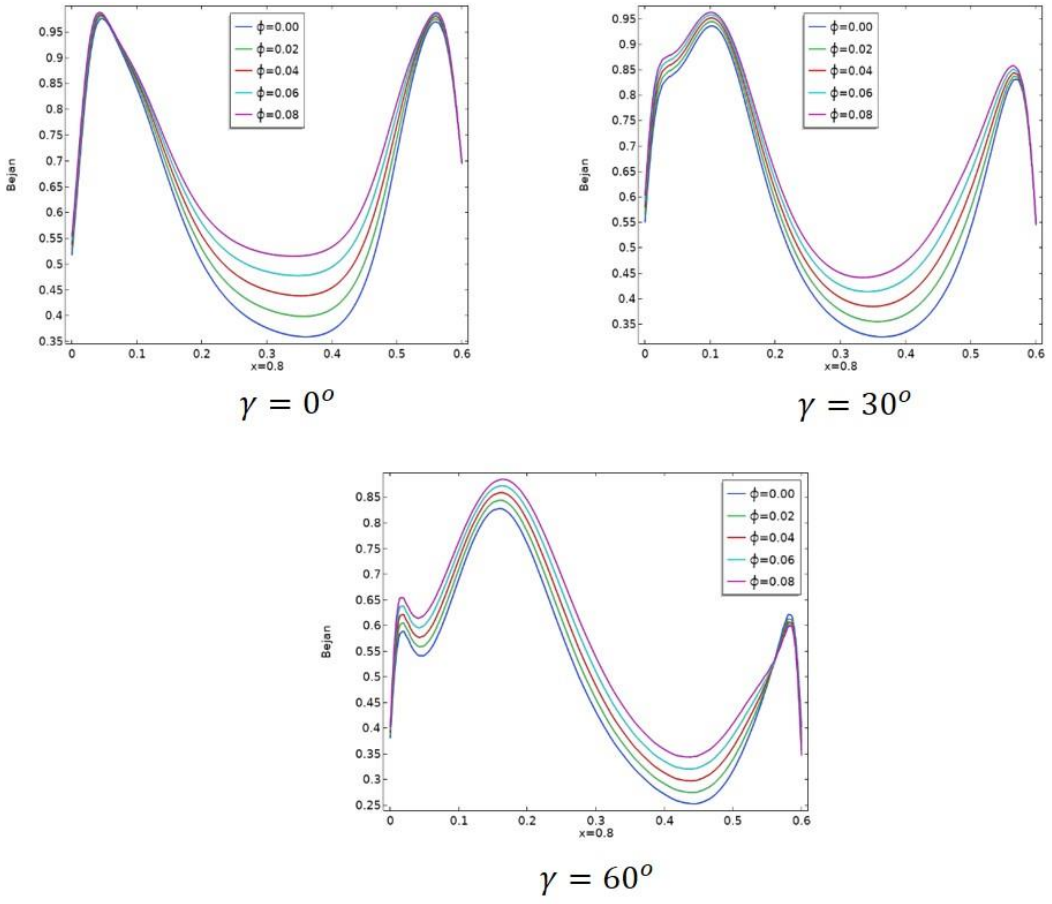


**Figure 6**. Impact on Bejan number for different $\phi$ with $Ha = 20$ and $Ra = 10^4$.

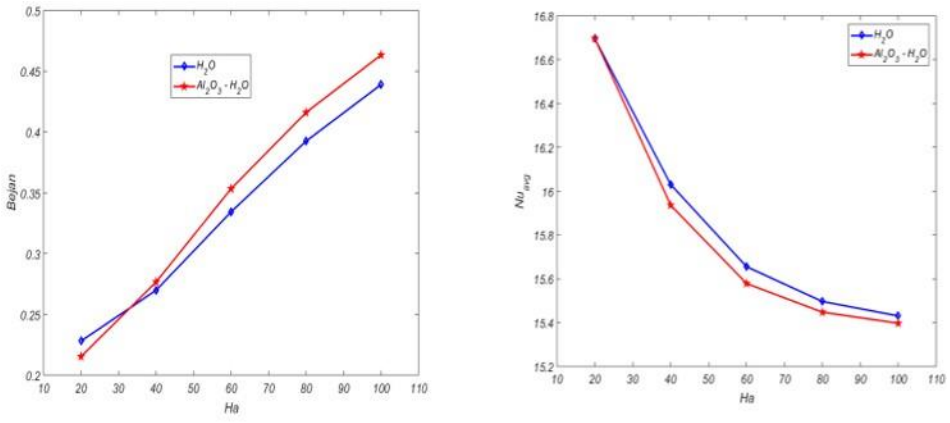


(a) Bejan number against $Ha$. (b) $Nu_{avg}$ against $Ha$

**Figure 7**. Impact on $Be_{avg}$ and $Nu_{avg}$ against $Ha$ for based fluid and nanofluid.

## 6. Conclusions

A thermal case study is designed to investigate the effect of inclination on MHD nanofluid on thermal flow field in a staggered cavity in presence of insulated baffles. Simulations have been carried out on various scales of the volume fraction $(0.00 \leq \phi \leq 0.08)$, Hartmann number $(0 \leq Ha \leq 100)$, Rayleigh number $(10^3 \leq Ra \leq 10^5)$, and inclination $(0^o \leq \gamma \leq 60^o)$. The obtained results can be concluded as:

- While keeping other parameters constant, raising the Rayleigh number $Ra$ improves heat transmission and flow strength.
- For larger values of volume fraction $(\phi)$ velocity admits significant increase.
- Isotherms reflects higher magnitude change towards positive variation in volume fraction $(\phi)$.
- Increasing Hartmann number $Ha$ leads to increase in average Bejan number $Be$.
- Average heat transfer rate $Nu_{avg}$ is decreasing function of Hartmann number $Ha$.

## Acknowledgements

The authors would like to thank Prince Sultan University for their support through the TAS research lab.

## Conflict of interest

The authors declare no conflict of interest.

## References

1. U. Ghia, K. N. Ghia, C. T. Shin, High-Re solutions for incompressible flow using the Navier-Stokes equations and a multigrid method, *J. Comput. Phys.*, **48** (1982), 387–411. https://doi.org/10.1016/0021-9991(82)90058-4
2. W. F. Spotz, G. F. Carey, High-order compact scheme for the steady stream-function vorticity equations, *Int. J. Numer. Methods Eng.*, **38** (1995), 3497–3512. https://doi.org/10.1002/nme.1620382008
3. J. C. Kalita, D. C. Dalal, A. K. Dass, A class of higher order compact schemes for the unsteady two-dimensional convection-diffusion equation with variable convection coefficients, *Int. J. Numer. Methods Fluids*, **38** (2002), 1111–1131. https://doi.org/10.1002/fld.263
4. J. C. Kalita, P. Chhabra, An improved (9, 5) higher order compact scheme for the transient two-dimensional convection-diffusion equation, *Int. J. Numer. Methods Fluids*, **51** (2006), 703–717. https://doi.org/10.1002/fld.1133
5. S. K. Pandit, J. C. Kalita, D. C. Dalal, A fourth-order accurate compact scheme for the solution of steady Navier-Stokes equations on non-uniform grids, **37** (2008), 121–134. https://doi.org/10.1016/j.compfluid.2007.04.002

6. P. M. Tekić, J. B. Rađenović, N. Lj. Lukić, S. S. Popović, Lattice Boltzmann simulation of two-sided lid-driven flow in a staggered cavity, **24** (2010), 383–390. https://doi.org/10.1080/10618562.2010.539974
7. Y. Bazilevs, M. Hsu, J. Kiendl, R. Wüchner, K. Bletzinger, 3D simulation of wind turbine rotors at full scale. Part II: Fluid-structure interaction modeling with composite blades, *Int. J. Numer. Methods Fluids*, **65** (2010), 236–253. https://doi.org/10.1002/fld.2454.
8. J. C. Kalita, B. B. Gogoi, Global two-dimensional stability of the staggered cavity flow with an HOC approach, *Comput. Math. Appl.*, **67** (2014), 569–590. http://doi.org/10.1016/j.camwa.2013.12.001
9. J. V. Indukuri, R. Maniyeri, Numerical simulation of oscillating lid driven square cavity, *Alexandria Eng. J.*, **57** (2018), 2609–2625. http://doi.org/10.1016/j.aej.2017.07.011
10. H. F. Oztop, E. Abu-nada, Numerical study of natural convection in partially heated rectangular enclosures filled with nanofluids, *Int. J. Heat Fluid Flow*, **29** (2008), 1326–1336. https://doi.org/10.1016/j.ijheatfluidflow.2008.04.009
11. M. Hinatsu, J. H. Ferziger, Numerical computation of unsteady incompressible flow in complex geometry using a composite multigrid technique, *Int. J. Numer. Methods Fluids*, **13** (1991), 971–997. https://doi.org/10.1002/fld.1650130804
12. H. C. Kuhlmann, M. Wanschura, H. J. Rath, Flow in two-sided lid-driven cavities: non-uniqueness, instabilities, and cellular structures, **336** (1997), 267–299. https://doi.org/10.1017/S0022112096004727
13. S. Albensoeder, H. C. Kuhlmann, H. J. Rath, Multiplicity of steady two-dimensional flows in two-sided lid-driven cavities, *Theor. Comput. Fluid Dyn.*, **14** (2001), 223–241.
14. Y. C. Zhou, B. S. V Patnaik, D. C. Wan, G. W. Wei, DSC solution for flow in a staggered double lid driven cavity, *Int. J. Numer. Methods Eng.*, **234** (2003), 211–234. https://doi.org/10.1002/nme.674
15. P. Nithiarasu, C. -B. Liu, Steady and unsteady incompressible flow in a double driven cavity using the artificial compressibility ( AC ) -based characteristic-based split ( CBS ) scheme, *Int. J. Numer. Methods Eng.*, **63** (2005), 380–397. https://doi.org/10.1002/nme.1280
16. S. A. M. Alsallami, Usman, S. U. Khan, A. Ghaffari, M. I. Khan, M. A. El-Shorbagy, et al., Numerical simulations for optimised flow of second-grade nanofluid due to rotating disk with nonlinear thermal radiation: Chebyshev spectral collocation method analysis, *Pramana-J. Phys.*, **96** (2022), 98. https://doi.org/10.1007/s12043-022-02337-8
17. Usman, A. A. Memon, H. Anwaar, T. Muhammad, A. A. Alharbi, A. S. Alshomrani, et al., A forced convection of water-aluminum oxide nanofluids in a square cavity containing a circular rotating disk of unit speed with high Reynolds number: A Comsol multiphysics study, *Case Stud. Therm. Eng.*, **39** (2022), 102370. https://doi.org/10.1016/j.csite.2022.102370
18. S. Eiamsa-ard, S. Pattanapipat, P. Promvonge, Influence of triangular wavy baffles on heat and fluid flow characteristics in a channel, **27** (2013), 2199–2208. http://doi.org/10.1007/s12206-013-0534-8
19. A. A. A. A. Al-Rashed, W. Aich, L. Kolsi, O. Mahian, A. K. Hussein, M. N. Borjini, Effects of movable-baffle on heat transfer and entropy generation in a cavity saturated by CNT suspensions: three-dimensional modeling, *Entropy*, **19** (2017), 200. https://doi.org/10.3390/e19050200

20. K. U. Rehman, N. Kousar, W. A. Khan, N. Fatima, On fluid flow field visualization in a staggered cavity: A numerical result, *Processes*, **8** (2020), 226. https://doi.org/10.3390/pr8020226
21. P. B. A. Reddy, T. Salah, S. Jakeer, M. A. Mansour, A. M. Rashad, Entropy generation due to magneto-natural convection in a square enclosure with heated corners saturated porous medium using Cu/water nanofluid, *Chinese J. Phys.*, **77** (2022), 1863–1884. https://doi.org/10.1016/j.cjph.2022.01.012
22. M. M. Bhatti, R. Ellahi, M. Hossein Doranehgard, Numerical study on the hybrid nanofluid ($Co_3O_4$-Go/$H_2O$) flow over a circular elastic surface with non-Darcy medium: Application in solar energy, *J. Mol. Liq*., **361** (2022), 119655. https://doi.org/10.1016/j.molliq.2022.119655
23. M. M. Bhatti, O. A. Bég, R. Ellahi, T. Abbas, Natural convection non-Newtonian EMHD dissipative flow through a microchannel containing a non-Darcy porous medium: Homotopy perturbation method study, *Qual. Theory Dyn. Syst.*, **21** (2022), 97.
24. S. Marzougui, F. Mebarek-Oudina, A. Assia, M. Magherbi, Z. Shah, K. Ramesh, Entropy generation on magneto-convective flow of copper-water nanofluid in a cavity with chamfers, *J. Therm. Anal. Calorim.*, **143** (2021), 2203–2214.
25. O. Mahian, A. Kianifar, C. Kleinstreuer, M. A. Al-Nimr, I. Pop, A. Z. Sahin, et al., A review of entropy generation in nanofluid flow, *Int. J. Heat Mass Transf.*, **65** (2013), 514–532. https://doi.org/10.1016/j.ijheatmasstransfer.2013.06.010
26. S. Lee, S. U. -S. Choi, S. Li, J. A. Eastman, Measuring thermal conductivity of fluids containing oxide nanoparticles, *Heat Transf.*, **121** (1999), 280–289. https://doi.org/10.1115/1.2825978
27. J. C. Maxwell, *A Treatise On Electricity and Magnetism*, Cambridge: Cambridge University Press, **2** (1873). https://doi.org/10.1017/CBO9780511709340
28. J. A. Templeton, R. E. Jones, J. W. Lee, J. A. Zimmerman, and B. M. Wong, A long-range electric field solver for molecular dynamics based on atomistic-to-continuum modeling, *J. Chem. Theory Comput.*, **7** (2011), 1736–1749. https://doi.org/10.1021/ct100727g
29. X. Liu, L. Liu, An immersed transitional interface finite element method for fluid interacting with rigid/deformable solid, *Eng. Appl. Comput. Fluid Mech.*, **13** (2019), 337–358. https://doi.org/10.1080/19942060.2019.1586774
30. R. Mahmood, N. Kousar, K. Ur. Rehman, M. Mohasan, Lid driven flow field statistics: A non-conforming finite element simulation, *Phys. A*, **528** (2019), 121198. https://doi.org/10.1016/j.physa.2019.121198
31. S. Bilal, R. Mahmood, A. H. Majeed, I. Khan, K. S. Nisar, Finite element method visualization about heat transfer analysis of Newtonian material in triangular cavity with square cylinder, *J. Mater. Res. Technol.*, **9** (2020), 4904–4918. https://doi.org/10.1016/j.jmrt.2020.03.010
32. M. Hatami, S. E. Ghasemi, Thermophoresis and Brownian diffusion of nanoparticles around a vertical cone in a porous media by Galerkin finite element method (GFEM), *Case Stud. Therm. Eng.*, 28 (2021), 101627. https://doi.org/10.1016/j.csite.2021.101627
33. X. F. Yang, X. M. He, A fully-discrete decoupled finite element method for the conserved Allen–Cahn type phase-field model of three-phase fluid flow system, *Comput. Methods Appl. Mech. Engrg.*, **389** (2022), 114376. https://doi.org/10.1016/j.cma.2021.114376

34. S. Maarouf, C. Bernardi, D. Yakoubi, Characteristics/finite element analysis for two incompressible fluid flows with surface tension using level set method, *Comput. Methods Appl. Mech. Engrg.*, **394** (2022), 114843. https://doi.org/10.1016/j.cma.2022.114843
35. S. Averweg, A. Schwarz, C. Schwarz, J. Schröder, 3D modeling of generalized Newtonian fluid flow with data assimilation using the least-squares finite element method, *Comput. Methods Appl. Mech. Engrg.*, **392** (2022), 114668. https://doi.org/10.1016/j.cma.2022.114668
36. A. D. Hobiny, I. Abbas, The impacts of variable thermal conductivity in a semiconducting medium using finite element method, *Case Stud. Therm. Eng.*, **31** (2022), 101773. https://doi.org/10.1016/j.csite.2022.101773


AIMS Press